Journal of Power Sources 248 (2014) 577–581

Contents lists available at ScienceDirect

Journal of Power Sources

journal homepage: www.elsevier.com/locate/jpowsour

Short communication

Fabrication of electrolyte-free fuel cell with $Mg_{0.4}Zn_{0.6}O/Ce_{0.8}Sm_{0.2}O_{2-\delta}$–$Li_{0.3}Ni_{0.6}Cu_{0.07}Sr_{0.03}O_{2-\delta}$ layer

Huiqing Hu [a], Qizhao Lin [a,*], Zhigang Zhu [a], Bin Zhu [b], Xianrong Liu [b]

[a] Department of Thermal Science and Energy Engineering, University of Science and Technology of China, Jinzhai Road, Hefei 230026, China
[b] Department of Energy Technology, Royal Institute of Technology, Stockholm S-100 44, Sweden

HIGHLIGHTS

- Electrolyte-free fuel cell (EFFC) in large cell size was produced.
- EFFC with the cell size of 1 cm in diameter demonstrated good cell performance.
- Low-cost raw materials (Mg and Zn) were introduced to EFFC for the first time.
- The EFFC we produced would be an optimum for the commercialization of EFFC.

ARTICLE INFO

Article history:
Received 13 June 2013
Received in revised form
6 September 2013
Accepted 22 September 2013
Available online 1 October 2013

Keywords:
Electrolyte-free fuel cell
Samarium doped ceria
Co-doped
Engineering cell
Dry pressing
Power density

ABSTRACT

Electrolyte-free fuel cell (EFFC) which holds the similar function with the traditional solid oxide fuel cell (SOFC) but possesses a completely different structure, has draw much attention during these years. Herein, we report a complex of MZSDC–LNCS ($Mg_{0.4}Zn_{0.6}O/Ce_{0.8}Sm_{0.2}O_{2-\delta}$–$Li_{0.3}Ni_{0.6}Cu_{0.07}Sr_{0.03}O_{2-\delta}$) for EFFC that demonstrates a high electrochemical power output of about 600 mW cm^{-2} at 630 °C. The co-doped MZSDC is synthesized by a co-precipitation method. Semiconductor material of LNCS is synthesized by direct solid state reaction. The microstructure and morphology of the composite materials are characterized by X-ray diffraction (XRD), scanning electron microscope (SEM) and energy-dispersive X-ray spectrometer (EDS). The performance of the cell with a large size (6 × 6 cm^2) is comparable or even better than that of the conventional solid oxide fuel cells with large sizes. The maximum power output of 9.28 W is obtained from the large-size cell at 600 °C. This paper develops a new functional nanocomposite for EFFC which is conducive to its commercial use.

1. Introduction

Solid oxide fuel cell (SOFC) is one of the most promising fuel cells because of its high efficiency in energy conversion, relatively low sensitivity to impurities and good fuel flexibility [1–3]. Conventional SOFC historically consists of three basic components which include a porous anode, a porous cathode and an electrolyte. And the electrolyte is used as a critical separation barrier to separate two electrodes [4,5].

Very recently, Electrolyte-free fuel cell (EFFC) which was proposed and developed as a revolutionary technology [6–9], has attracted great attention. The electrolyte layer, which is a bottleneck of the conventional SOFC technology, has been physically replaced by a unique single homogeneous multifunctional nanocomposite layer in EFFC. It is amazing to find that this novel device, integrating the functions of anode, electrolyte and cathode of the classic three-component structure SOFC, can still realize the function of fuel cell [10–13] and not show short-circuit problem. The nanocomposite used in EFFC has two basic phases which are an ionic conductor and a semiconductor which provide percolating paths for ions and electrons respectively. The ionic conductors are usually $Sm_{0.2}Ce_{0.8}O_{1.9}$ (SDC) and $Ce_{0.9}Gd_{0.1}O_{1.9}$ (GDC). The semiconductors which work as binary catalysts for hydrogen oxidation reaction (HOR) and oxygen reduction reaction, are normally transition metal oxides such as NiO, CuO, ZnO and FeO_x [14]. It has been proposed that the schematic illustration for conventional SOFC and EFFC can be understood in Fig. 1(a) and (b), respectively.

The working mechanism of the EFFC is different from the conventional SOFC which can be described below:

* Corresponding author. Tel.: +86 551 63602487.
E-mail addresses: huhq@mail.ustc.edu.cn (H. Hu), qlin@ustc.edu.cn (Q. Lin).

0378-7753/$ – see front matter © 2013 Elsevier B.V. All rights reserved.
http://dx.doi.org/10.1016/j.jpowsour.2013.09.095

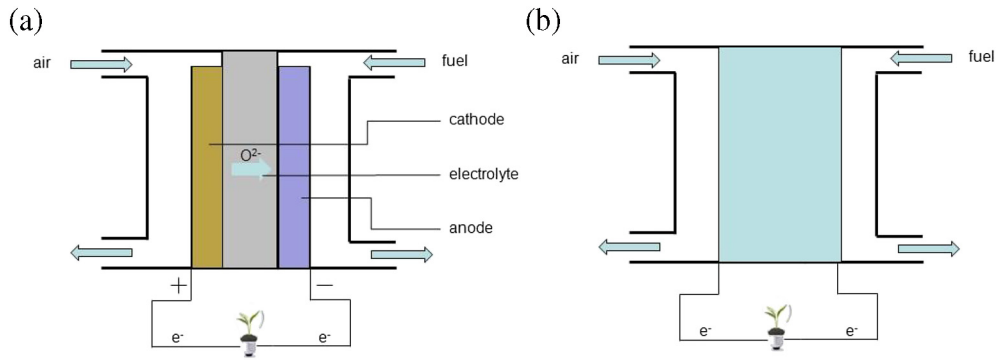

Fig. 1. Schematic illustration of (a) a conventional three-component SOFC and (b) EFFCEFC.

Anode:

$$H_2 \rightarrow 2H^+ + 2e^-$$

Cathode:

$$\frac{1}{2}O_2 + 2e^- \rightarrow O^{2-}$$

Overall reaction:

$$H_2 + \frac{1}{2}O_2 \rightarrow H_2O$$

The studies on EFFC mainly focused on the basic and fundamental issues such as redox reaction activities and investigation of the operation mechanism in the past few years. In this work, we continue to study this new energy device and mainly focus on the development of new type and cost-effective materials for EFFC which show good performance for practical applications. The single cell using the composite was fabricated and studied by the microstructure analysis on the as-prepared sample. Moreover, the power output of the fuel cells was measured. For the first time, we made use of Zn and Mg in EFFC to reduce the cost and produced the single cell which showed good performance with a large size (6×6 cm^2) to meet the demands for practical applications.

2. Experimental

2.1. Synthesis of the MZSDC–LNCS ($Mg_{0.4}Zn_{0.6}O/Ce_{0.8}Sm_{0.2}O_{2-\delta}$–$Li_{0.3}Ni_{0.6}Cu_{0.07}Sr_{0.03}O_{2-\delta}$) powder

Preparation of MZSDC. MZSDC was prepared by one-step co-precipitation technique as reported elsewhere [18]. $Mg(NO_3)_2 \cdot 6H_2O$, $Zn(NO_3)_2 \cdot 6H_2O$, $Ce(NO_3)_3 \cdot 6H_2O$ and $Sm(NO_3)_3 \cdot 6H_2O$ were dissolved in deionic water with an optimal molar ratio of Mg:Zn:Ce:Sm = 0.12:0.18:0.55:0.14 to form a solution with concentration of 0.1 mol L^{-1}. Then Na_2CO_3 solution of 0.2 mol L^{-1}, used as a precipitation agent, was added dropwise under vigorous stirring for 30 min to form a white precipitation. The precipitate was then washed, filtrated and dried in the oven at room temperature for 24 h and sintered in a furnace at 700 °C for 4 h. The resulting material was then completely ground in a mortar to generate MZSDC composite powder.

Preparation of LNCS. Semiconductor material of $Li_{0.3}Ni_{0.6}Cu_{0.07}Sr_{0.03}O_{2-\delta}$ (LNCS) was synthesized by direct solid state reaction method. Stoichiometric amounts of Li_2CO_3, $NiCO_32Ni(OH)_2 \cdot 4H_2O$, $CuCO_3 \cdot Cu(OH)_2 \cdot H_2O$ and $SrCO_3$ were mixed and ground with a molar ratio of Li:Ni:Cu:Sr = 0.3:0.6:0.07:0.03 in a mortar, then the mixture was sintered at 800 °C for 2 h and then ground completely.

The MZSDC–LNCS powder was prepared by mixing the above MZSDC and LNCS powder with the weight ratio of 4:3. The mixture was wet milled in organic medium for 48 h using a ball milling machine, and then heated at 700 °C for 2 h.

2.2. Cell fabrication

A fuel cell was fabricated by a dry pressing method. The small size cell was fabricated with an active area of 0.64 cm^2 (13 mm in diameter and 0.80 mm in thickness). The large size cell was fabricated by pressing the prepared mixture powder with a pressure of 100–300 MPa to form the tablet. The large size cell was fabricated with an active area of 25 cm^2 (1 mm in thickness). Then the cells were hot-pressed under 30 tons at 650 °C for 120 min to form a dense plate with enough mechanical strength. The external surfaces of the electrodes were fabricated by copper grating and silver paste for the large size and small size cell respectively, which act as the current collectors to achieve good *I–V* and *I–P* characteristics for the fuel cells.

2.3. Characterization of the MZSDC–LNCS powder and the small size cell

The crystal structure of the as-prepared composite material was analyzed by X-ray diffraction (XRD) using Rigaku-D/Max-3A diffractometer with Cu-Kα radiation. The XRD spectra were recorded from 20° to 80° at a scan speed of 8°/min. The morphology of the samples was studied with a Zeiss Ultra 55 field emission scanning electron microscopy (FE-SEM). Components of the small size cell were identified by the energy dispersive X-ray spectrometer (EDX) analyzer (XP30, Philips).

The electrical conductivity of the small size cell was measured in air by A.C. impedance spectroscopy method in a temperature range of 300–650 °C using an electrochemical work station (CHI660B, Cheng Hua Corp.), and the measurement was performed in the frequency ranging from 1 Hz to 100 kHz with a bias voltage of 5 mV.

2.4. Fuel cell performance

The electrochemical performance of the fuel cells was tested at 530–650 °C by a computer integrated instrument, where hydrogen and air were used as the fuel and oxidant respectively. The gas flow rates was in the range of 80–110 sccm for the small size cell and 1000–2000 ml for the large size cell at 1 atm pressure. The electrochemical performance of the cell with large size was recorded at temperature of 600 °C.

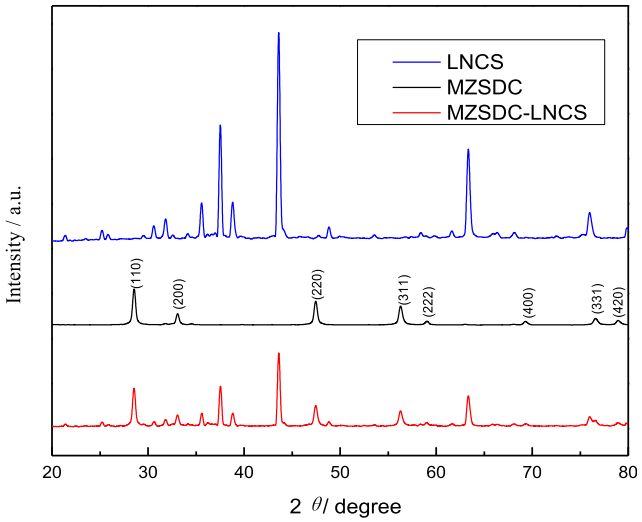

Fig. 2. XRD diffraction patterns of the individual MZSDC and LNCS powders.

3. Results and discussion

3.1. Phase analysis and crystal structure

Fig. 2 shows the XRD patterns of the as-prepared samples. The XRD pattern of MZSDC is similar to that of pure CeO_2, only the 2θ values slightly shift toward the relatively higher angles. It contains a cubic fluorite structure of CeO_2 (JCPDS No. 81-0792). No individual phase of Sm_2O_3, MgO or ZnO can be detected, which shows that Sm^{3+}, Zn^{2+} and Mg^{2+} have been co-doped into ceria. The index of crystal lattice increases due to the substitution of Ce^{4+} with Sm^{3+}, Zn^{2+} and Mg^{2+} in the lattice of CeO_2 [15]. As reported in previous work [16], using the above preparation method, a doped ceria-Na_2CO_3 two-phase composite can be formed which is same to that of SDC–Na_2CO_3 composite. The Na_2CO_3 was amorphously distributed, since no peak was observed. As for the XRD pattern of LNCS, two different series of diffraction patterns are observed, which can be ascribed to LiNiO and CuO, respectively. XRD pattern of Sr-containing compound cannot be observed due to the very little content of Sr. The XRD pattern of MZSDC–LNCS composite showed that it is a mixture of LNCS and MZSDC phases. No other phase can be found, indicating that there is no obvious interaction between LNCS and MZSDC.

3.2. Microstructure and morphology

Fig. 3(a) shows the photograph of an as-prepared fuel cell of large size. The single cell has an effective area of 25 cm^2 with the thickness of 1 mm. The SEM results present the microstructure information of the as-prepared MZSDC sample and LNCS sample as shown in Fig. 3(b) and (c). The particle size and morphology of the as-prepared samples can be modulated by the preparation parameters, especially the sintering temperature and reaction time. The particle size of MZSDC ranges from tens of nanometers to several hundreds of nanometers. For LNCS, the particle size is in the range of several hundred nanometers to micrometers and the sample is heavily agglomerated due to the high sintering temperature. EDS can measure the local chemical composition of the samples due to the compactness, efficiency and sensitivity [17]. The EDS results show that the nanostructure and morphology of the particle are uniform. Fig. 4 shows the EDS spectrum of the elements in the single cell in detail. The figures show the presence of Ce, Sm, Mg, Zn, Ni, Cu and Sr peaks. To gain further insight into the chemical composition of the particles, Fig. 5 presents the elemental mapping of the MZSDC–LNCS pellet. It should be noticed that MZSDC–LNCS sample has an evenly distributed MZSDC and LNCS particles, which will be helpful to enhance the performance of the cell.

3.3. AC impedance and electrical conductivity

Fig. 6 presents the electrochemical impedance spectroscopy (EIS) and the corresponding equivalent circuit of the cell. The equivalent circuit was simulated by software of ZSIM in order to find the internal resistances of the cell. The frequency in measurements is ranging from 1 MHz to 0.1 Hz via tailoring the voltage at different temperatures. The EIS result shows the same feature which is a "semicircle" in low frequency followed by a "tail". Based on the small intercept at the real axis of the "semicircle portion". It can be concluded that both the reactions for H_2 and O_2 are fast kinetic processes. This conclusion implies that a mixed MZSDC–LNCS homogenous material has the high catalytic activity for both H_2 and O_2. In the equivalent circuit, R1 denotes the ohmic resistance which is mainly caused by the oxygen ions and electrons. In this case, the ohmic resistance contains both of the contributions from the electrons and ions. R2Q and R3Q denote the charge transfer and mass transfer resistances, respectively. L indicates the effect of stainless tube in the testing device. In addition, arcs in the spectra of the sample shrink as the measurement temperature increases from 300 °C to 600 °C. The results can reflect that the overall resistance of the cell is decreased with increasing temperature.

The electrical conductivity of the as-prepared sample is further calculated based on the EIS results. The electrical conductivity is gradually increased from 300 °C to 600 °C. The total conductivity reaches the maximum of about 0.1 S cm^{-1} at 600 °C. It was reported that dopant with a suitable concentration is necessary to get the optimum conductivity [18]. The introduction of alkaline earth ions into co-doped ceria can also result in the improvement of ionic conductivity in the as-prepared sample [19]. The deliberate choice of LNCS weight ratio for the sample will lead to suitable electrons production in the cell. Both the ionic MZSDC and electronic LNCZ phases contribute to the electrical conductivity due to their co-existence in the complex. The reaction in single cell will be enhanced because of the high ionic conductivity.

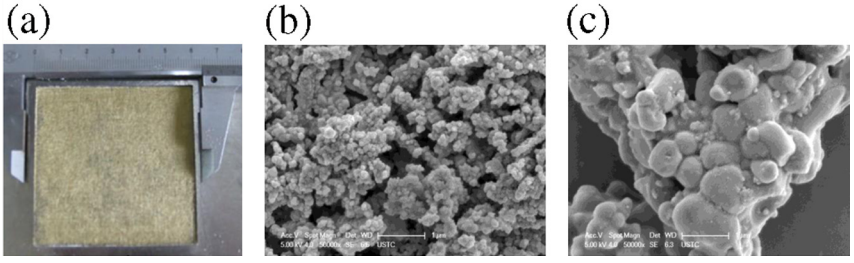

Fig. 3. (a) Photo of the as-prepared cell; FE-SEM images of the individual (b) MZSDC and (c) LNCS powders.

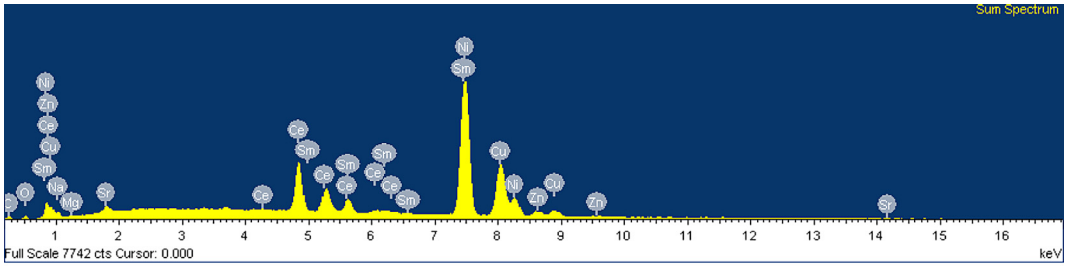

Fig. 4. EDS spectrum of MZSDC–LNCS component.

3.4. Cell performance

Zn and Mg were introduced into the ionic conductor part in single fuel cell which can maintain the good output performance and reduce the overall cost of the fuel cell simultaneously. The well-connected Mg and Zn also contribute to the high performance of the fuel cell. Zinc oxide and magnesium oxide have drawn much attention in the SOFC research because of their abundant availability, low cost, thermal and chemical stability, and high electrical conductivity at both reducing and oxidizing atmospheres [20]. It was reported that a doped ceria in composite with zinc oxide can improve the electrical conductivity [21] and Mg can be used to improve the grain-boundary conduction in SOFC [22]. One function of MgO and ZnO in MZSDC is to alter the electronic states of these particles for improvement of the catalytic activity [23]. And the other one is that the introduction of $Mg(NO_3)_2{\cdot}6H_2O$ and $Zn(NO_3)_2{\cdot}6H_2O$ which were used to partly replace the rare earth materials of $Ce(NO_3)_3{\cdot}6H_2O$ and $Sm(NO_3)_3{\cdot}6H_2O$ in fuel cell, will reduce the cost of whole device. The introduction of Sr can increase the electrical conductivity, improve the operational stability and lead to good cell performance for EFFC due to the greater amount of electronic holes originated from the increased interstitial oxygen species [24,25]. MZSDC is an oxygen ionic conductor, while the metal oxides (NiO and CuO) have shown high catalytic activity for both hydrogen oxidation reaction and oxygen reduction reaction [26]. It is well known that Li^+ doped NiO is a p-type semiconductor, while CuO is an n-type semiconductor. Thus a p–n junction may be formed within LNCS to keep an effective charge separation to block the internal electronic conduction in EFFC when exposed to H_2 and/or O_2 atmosphere [7]. Therefore, the as-prepared MZSDC–LNCS can satisfy the material requirement for EFFC which has the potential for commercialization.

Performance of the fuel cell of small size is shown in Fig. 7. It is found that the power density increases when the operating temperature increases. The maximum power density (P_{max}) of the cell, using H_2 as the fuel, reaches the maximum of about 600 mW cm^{-2} at 650 °C, which is 402 mW cm^{-2} at 530 °C. The open-circuit voltage (OCV) is 1.08 V at 650 °C. The electrode polarization process is not evident as indicated by the near linear characteristics of the *I–V* curve in Fig. 7. The LNCS/MZSDC material is a new type material for EFFC, which has demonstrated a good device performance with power density of 9.28 W (371 mW cm^{-2}) obtained

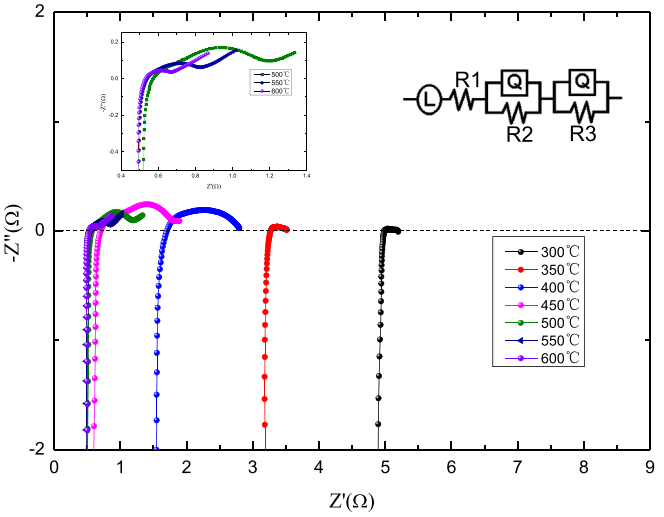

Fig. 6. Electrochemical Impedance spectra and the corresponding equivalent circuit of the cell pellet.

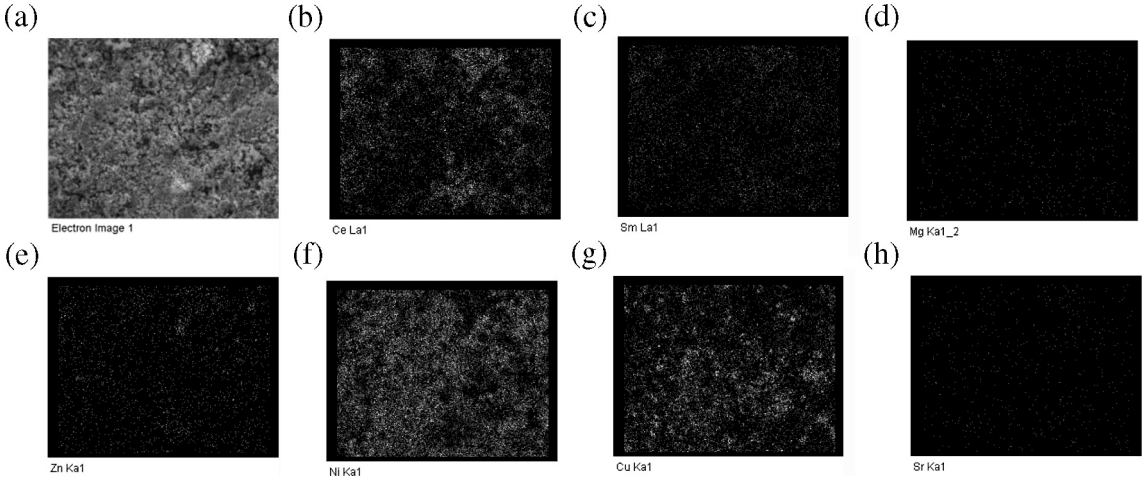

Fig. 5. (a)FE-SEM micrographs of the MZSDC–LNCS powder,(b) Ce, (c) Sm, (d) Mg, (e)Zn, (f)Ni, (g) Cu and (h) Sr elemental mappings of the MZSDC–LNCS powder. The mapping regions are showed in Fig. 4(a).

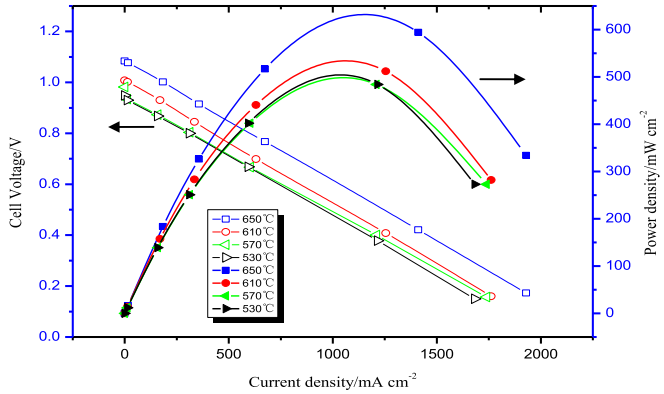

Fig. 7. *I–V/I–P* characteristics of the small size fuel cell at different temperatures.

Table 1
The cell performance of the EFFC with large size.

OCV/V	Load			
	Current/A	Voltage/V	Power/W	Power density/mW cm^{-2}
1.02	11.6	0.8	9.28	371

from a large size device at 600 °C (Table 1). The reported performances of single cell for EFFC are commonly based on small sizes (less than 1 cm^2) and the power output is usually less than 1 W [8–11,26]. The P_{max} of EFFC reported by Zhu et al. was 600 mW cm^{-2} and 450 mW cm^{-2} when using $LiNiZnO_{2-\delta}$–SDC mixed layer and $LiNiO_2$–GDC composite material, respectively, and the measurement temperature is 550 °C [6,7]. In this work, we fabricate both the large size and the small size cells at the same time. As can be seen from Table 1 and Fig. 6, the P_{max} of large size cell at 600 °C is much lower than that of small size cell. As reported in literature, cell of large size will cause significant loss to the power density. The P_{max} of the cell with size of 4.1 × 4.1 cm^2 is 303 mW·cm^{-2} at 550 °C, as reported by Lin et al. [27]. There are very few reports on the subject of fabricating large size cells for EFFC in recent years. The present work has contributed to the development in the field, which will help to the commercialization of EFFC in the future.

4. Conclusions

In this study, we have fabricated an EFFC in which homogeneous material of MZSDC–LNCS is used as the single-component oxide layer. The total resistance of the cell is decreased with increasing temperature. The fuel cell is fabricated as a practical engineering cell which shows the promising performance. The maximum power density of the cell with a small size is about 600 mW cm^{-2} at 630 °C when H_2 and air are used as the fuel and the oxidant, respectively. The maximum power of 9.28 W, which is obtained from a large size EFFC (6 × 6 cm^2) at 600 °C, was comparable or even better than that of the conventional solid oxide fuel cells with large sizes. The EFFC shows good performance with low cost, which has great potential for the commercial application in the future.

Acknowledgments

This work was supported by National Key Basic Research Program (No. 2010CB227300) founded by MOST, National Natural Science Foundation of China (No. 51376171) and Swedish Research Council (VR, No. 621-2011-4983), European Commission FP7 Tri-SOFC project (No. 303454).

References

[1] W. Grove, Philos. Mag. Ser. 314 (1839) 127.
[2] D. Mat, X. Liu, Z. Zhu, B. Zhu, Int. J. Hydrogen Energy 32 (2007) 796.
[3] S. Park, J.M. Vohs, R.J. Gorte, Nature 400 (1999) 649.
[4] S. Toshio, H. Zahir, F. Yoshihiro, Y. Toshiaki, F. Yoshinobu, A. Masanobu, Nature 325 (2009) 852.
[5] B.C. Steele, A. Heinzel, Nature 414 (2001) 345.
[6] B. Zhu, Y. Ma, X. Wang, R. Raza, H.Y. Qin, L.D. Fan, Electrochem. Commun. 13 (2011) 225.
[7] B. Zhu, R. Raza, G. Abbas, M. Singh, Adv. Funct. Mater. 21 (2011) 2465.
[8] B. Zhu, R. Raza, H.Y. Qin, Q. Liu, L.D. Fan, Energy Environ. Sci. 4 (2011) 2986.
[9] B. Zhu, R. Raza, Q. Liu, H.Y. Qin, Z.G. Zhu, RSC Adv. 2 (2012) 5066.
[10] B. Zhu, H.Y. Qin, R. Raza, Q. Liu, L.D. Fan, J. Patakangas, Int. J. Hydrogen Energy 36 (2011) 8536.
[11] B. Zhu, R. Raza, H.Y. Qin, L.D. Fan, J. Power Sources 196 (2011) 6362.
[12] H.Y. Qin, B. Zhu, R. Raza, M. Singh, L.D. Fan, P. Lund, Int. J. Hydrogen Energy 37 (2012) 19365.
[13] B. Zhu, L.D. Fan, L. Peter, Appl. Energy 106 (2013) 163.
[14] Y. Xia, X. Liu, Y. Bai, H. Li, X. Deng, X. Niu, X. Wu, D. Zhou, M. Lv, Z. Wang, Z. Meng, RSC Adv. 2 (2012) 3828.
[15] Y. Zheng, Y. Shi, H. Gu, L. Gao, H. Chen, L. Guo, Mater. Res. Bull. 44 (2009) 1717.
[16] R. Raza, X.D. Wang, Y. Ma, B. Zhu, Int. J. Hydrogen Energy 35 (2010) 2684.
[17] A.L. Soldati, L. Baque, H. Troiani, C. Cotaro, A. Schreiber, A. Caneiro, Int. J. Hydrogen Energy 36 (2011) 9180.
[18] R. Raza, X.D. Wang, Y. Ma, B. Zhu, J. Power Sources 195 (2010) 6491.
[19] J. Katayama, K. Ito, M. Matsuoka, J. Tamaki, J. Appl. Electrochem. 34 (2004) 687.
[20] W. Zhu, S. Deevi, Mater. Sci. Eng. 348 (2003) 227.
[21] J. Fergus, Solid State Ionics 171 (2004) 1.
[22] S. Deshpande, S. Patil, S. Kuchibhatla, S. Seal, Appl. Phys. Lett. 87 (2005) 1.
[23] R. Raza, X.D. Wang, Y. Ma, B. Zhu, J. Power Sources 195 (2010) 8067.
[24] A. Jun, J. Kim, J. Shin, Int. J. Hydrogen Energy 37 (2012) 18381.
[25] A. Hammouche, E. Siebert, A. Hammou, Mater. Res. Bull. 24 (1989) 367.
[26] X.D. Wang, Y. Ma, S. Li, A.H. Kashyout, B. Zhu, J. Power Sources 196 (2011) 2754.
[27] T. Lin, M. Lee, R. Yang, J. Chang, W. Kao, Mater. Lett. 81 (2012) 185.